



● *Original Contribution*

## ULTRAFAST MICROSCOPY IMAGING OF ACOUSTIC CLUSTER THERAPY BUBBLES: ACTIVATION AND OSCILLATION

ANNEMIEKE VAN WAMEL,<sup>\*</sup> MELINA MÜHLENPFORDT,<sup>\*</sup> RUNE HANSEN,<sup>†,‡</sup> ANDREW HEALEY,<sup>§</sup>  
FLODELIZA S. VILLANUEVA,<sup>¶</sup> SPIROS KOTOPOULIS,<sup>\*,||</sup> CATHARINA DE LANGE DAVIES,<sup>\*</sup> and XUCAI CHEN<sup>¶</sup>  
<sup>\*</sup>Department of Physics, Norwegian University of Science and Technology, Trondheim, Norway; <sup>†</sup>Department of Health Research, SINTEF Digital, Trondheim, Norway; <sup>‡</sup>Department of Circulation and Medical Imaging, Norwegian University of Science and Technology, Trondheim, Norway; <sup>§</sup>EXACT Therapeutics, Oslo, Norway; <sup>¶</sup>Center for Ultrasound Molecular Imaging and Therapeutics, University of Pittsburgh, Pittsburgh, Pennsylvania, USA; and <sup>||</sup>Department of Clinical Medicine, University of Bergen, Bergen, Norway

(Received 8 September 2021; revised 15 February 2022; in final form 10 May 2022)

**Abstract**—Acoustic Cluster Therapy (ACT<sup>®</sup>) is a platform for improving drug delivery and has had promising pre-clinical results. A clinical trial is ongoing. ACT<sup>®</sup> is based on microclusters of microbubbles–microdroplets that, when sonicated, form a large ACT<sup>®</sup> bubble. The aim of this study was to obtain new knowledge on the dynamic formation and oscillations of ACT<sup>®</sup> bubbles by ultrafast optical imaging in a microchannel. The high-speed recordings revealed the microbubble–microdroplet fusion, and the gas in the microbubble acted as a vaporization seed for the microdroplet. Subsequently, the bubble grew by gas diffusion from the surrounding medium and became a large ACT<sup>®</sup> bubble with a diameter of 5–50  $\mu\text{m}$ . A second ultrasound exposure at lower frequency caused the ACT<sup>®</sup> bubble to oscillate. The recorded oscillations were compared with simulations using the modified Rayleigh–Plesset equation. A term accounting for the physical boundary imposed by the microchannel wall was included. The recorded oscillation amplitudes were approximately 1–2  $\mu\text{m}$ , hence similar to oscillations of smaller contrast agent microbubbles. These findings, together with our previously reported promising pre-clinical therapeutic results, suggest that these oscillations covering a large part of the vessel wall because of the large bubble volume can substantially improve therapeutic outcome. (E-mail: [catharina.davies@ntnu.no](mailto:catharina.davies@ntnu.no)) © 2022 The Author(s). Published by Elsevier Inc. on behalf of World Federation for Ultrasound in Medicine & Biology. This is an open access article under the CC BY license (<http://creativecommons.org/licenses/by/4.0/>).

**Key Words:** Acoustic cluster therapy, Ultrafast microscopy imaging, Oscillations, Ultrasound contrast agent, Drug delivery.

### INTRODUCTION

Ultrasound contrast agents are stabilized gas microbubbles (typically 1–10  $\mu\text{m}$  in diameter). After intravenous injection, such microbubbles are stable for up to 2–3 min *in vivo* with no known side effects, other than potential allergic reactions. Microbubbles in combination with focused ultrasound have been reported to improve the delivery of drugs and nanoparticles in solid tumors in pre-clinical (Yan et al. 2013; Snipstad et al. 2017) and clinical (Dimcevski et al. 2016) studies, as well as temporarily increase the permeability of the blood–brain barrier (Tung et al. 2011;

Poon et al. 2017). On application of ultrasound, these microbubbles oscillate volumetrically in the vasculature and induce biomechanical effects that increase the permeability of the vascular wall and improve extravasation of drugs (Lajoinie et al. 2016; Yang et al. 2020). The microbubbles interact with nearby cells, probably forming small transient pores in the cell membrane via mechanical disruption in a process called sonoporation; microbubbles have even been observed to enter cells *in vitro* (Delalande et al. 2013; Yang et al. 2020). This interaction allows increased intracellular drug uptake in cells in proximity to the oscillating microbubbles. Furthermore, the oscillating microbubbles improve the penetration of therapeutic agents into the extracellular matrix (Delalande et al. 2013; Hussein et al. 2014; Lentacker et al. 2014; Lee et al. 2017; Qin et al. 2018; Roovers et al. 2019).

Address correspondence to: Catharina de Lange Davies, Department of Physics, Norwegian University of Science and Technology, Høgskoleringen 5, 7491 Trondheim, Norway. E-mail: [catharina.davies@ntnu.no](mailto:catharina.davies@ntnu.no)

Whereas various drug delivery approaches exploring the use of ultrasound and microbubbles have shown some promise, several issues hamper the effectiveness. Being small, the magnitude of the biomechanical work the microbubble can induce is limited, and being free flowing, they display limited contact with the endothelial wall, reducing the level and range of the biomechanical effects (Delalande *et al.* 2013; Kooiman *et al.* 2014). To produce enough biomechanical work, microbubbles often need a high ultrasound pressure that could induce inertial cavitation, with ensuing safety issues (Goertz 2015). To address the current limitations of microbubbles for drug delivery, a range of novel microbubble technology platforms are being developed, for example, cationic microbubbles (Delalande *et al.* 2017), monodisperse microbubbles (Pulsipher *et al.* 2018) and targeted microbubbles (Wang *et al.* 2018). A review of novel microbubbles has recently been published (Stride *et al.* 2020).

Acoustic Cluster Therapy (ACT, EXACT Therapeutics AS, Oslo, Norway) is a novel concept for ultrasound-mediated, localized drug delivery (Sontum *et al.* 2015; Myhre *et al.* 2016). ACT<sup>®</sup> is a formulation combining negatively charged microbubbles, stabilized by a monomolecular phospholipid membrane of hydrogenated egg phosphatidylserine with positively charged microdroplets containing perfluoromethylcyclopentane. A mixture of these microbubbles and microdroplets results in small microbubble–microdroplet clusters held together by the electrostatic forces. These microclusters can contain a single or a few microdroplets surrounded by a few microbubbles (Sontum *et al.* 2015). The ACT<sup>®</sup> microcluster dispersion is intended for co-administration with a therapeutic drug. When ACT<sup>®</sup> clusters are insonated with pulsed ultrasound (in the clinical diagnostic regime), the oscillating microbubbles transfer energy to the microdroplet, initiating vaporization and resulting in the formation of larger ACT<sup>®</sup> bubbles (Sontum *et al.* 2015). This first step in ultrasound-induced ACT<sup>®</sup> bubble generation is referred to as the activation step. *In vivo* studies have reported that the transition from microclusters to large ACT<sup>®</sup> bubbles can be achieved using ultrasound frequencies of 0.5 to 8 MHz (Healey *et al.* 2016; van Wamel *et al.* 2016a; Kotopoulis *et al.* 2017; Bush *et al.* 2020). Although a small, enhanced drug uptake was observed after this first step, a subsequent ultrasound exposure resulted in a considerably increased drug uptake, indicating that both the activation step and the subsequent sonication called the enhancement step are required (van Wamel *et al.* 2016a; Olsman *et al.* 2021). During the enhancement step, the ACT<sup>®</sup> bubbles are exposed to low-frequency (0.3–1.0 MHz) ultrasound at low pressures causing the ACT<sup>®</sup> bubbles to oscillate (Sontum *et al.* 2015; Healey *et al.*

2016). The ACT<sup>®</sup> bubbles are reported to have a diameter in the range 10–40  $\mu\text{m}$  and to form ellipsoidal bubbles, which are trapped in a small fraction of the microcirculation of 5–10 min (Sontum *et al.* 2015; van Wamel *et al.* 2016a). ACT<sup>®</sup> bubbles have a volume three orders of magnitude larger than that of conventional microbubbles used as contrast agents for ultrasound imaging and, therefore, have biomechanical effects, such as microstreaming and shear stress, on a larger segment of the capillary wall and have a potentially larger impact on local drug delivery. All constituents in the ACT<sup>®</sup> formulation are chemically and biologically inert; hence the mechanism is fully based on physical and biomechanical effects. No adverse effects of ACT<sup>®</sup> were found in pre-clinical testing in dogs and rats (Myhre *et al.* 2016). It should be emphasized that the ACT<sup>®</sup> bubbles lodge in a small fraction of the capillaries. Compared with regular microbubbles and ultrasound, rather low acoustic pressures are needed to obtain an enhanced therapeutic effect. The long residence time of the ACT<sup>®</sup> bubbles in the vasculature makes the bubbles powerful imaging agents, and contrast enhancement has been reported to correlate with therapeutic outcome (Bush *et al.* 2020), hence predicting the therapeutic performance.

Applying ultrasound toward the trapped ACT<sup>®</sup> bubbles in the tumor facilitates a localized delivery of co-injected drugs. Athymic mice with subcutaneously growing prostate tumors were treated with ACT<sup>®</sup> together with paclitaxel (Abraxane), and 120 days after treatment, the survival rate was 100%, compared with 0% in mice receiving Abraxane only (van Wamel *et al.* 2016b). Mice with orthotopically growing triple-negative breast cancer were treated with ACT<sup>®</sup> and doxorubicin (Doxil), and 180 days after treatment, 63% of the mice were in complete and stable remission, compared with 10% of the mice receiving Doxil only (Bush *et al.* 2020). Mice with subcutaneously growing pancreatic tumors treated with paclitaxel and ACT<sup>®</sup> exhibited reduced tumor growth compared with those treated with paclitaxel alone (Kotopoulis *et al.* 2017). ACT<sup>®</sup> has also been reported to temporarily increase the permeability of the blood–brain barrier, allowing polymeric nanoparticles to enter the brain parenchyma (Aslund *et al.* 2017; Olsman *et al.* 2021). A clinical study has been initiated in which liver metastases of colorectal cancer patients are being treated with standard chemotherapy combined with ACT<sup>®</sup> (ClinicalTrials.gov identifier: NCT04021277).

To optimize these successful therapeutic responses, knowledge of the behavior of ACT<sup>®</sup> bubbles is needed. Thus, the dynamics of ACT<sup>®</sup> bubble activation and volumetric oscillations at several frequencies and pressures

were recorded in microchannel of polydimethylsiloxane (PDMS), using ultrafast-frame-rate microscopy. To investigate whether the ACT<sup>®</sup> bubble oscillations followed the classic model for free bubble oscillation, the recorded oscillations were fitted to the modified Rayleigh–Plesset equation (Versluis et al. 2020). A term accounting for the presence of the wall of the microchannel was included to model the deviation from free space situation.

## METHODS

### *ACT agent preparation*

The ACT<sup>®</sup> microbubble–microdroplet cluster dispersion (PS101) was provided by EXACT Therapeutics AS. PS101 was prepared by reconstituting a freeze-dried suspension of microbubbles of perfluorobutane (PFB, F2 Chemicals Ltd., Lea Town, Preston, UK; 16  $\mu\text{L}/\text{vial}$ ) with a microdroplet emulsion of perfluoromethylcyclopentane (PFMCP, F2 Chemicals Ltd.; 6.8 mg/mL), dispersed in a 5 mM tris(hydroxymethyl)aminomethane (TRIS) buffer, forming a 2-mL dispersion (Sontum et al. 2015; Healey et al. 2016). The microbubbles were stabilized by a monomolecular phospholipid membrane of hydrogenated egg phosphatidylserine (H-EPS), which is negatively charged, embedded in an amorphous sucrose

structure. The microdroplets were stabilized by a monomolecular distearoylphosphatidylcholine (DSPC) phospholipid membrane containing 3% (mol/mol) stearyl amine, making the overall surface positively charged. The reconstituted PS101 formulation consists of a suspension of small microbubble–microdroplet conjugates (micro-clusters) at  $47 \times 10^6$  clusters/mL, with a median diameter of 5.6  $\mu\text{m}$ . The content of perfluoromethylcyclopentane, which is defined as the active pharmaceutical ingredient in PS101, is 6.5 mg/mL PS101, which was diluted in under saturated normal saline (0.9%) prior to use.

### *Microfluidic devices*

Microfluidic devices were made with PDMS (Sylgard 184 Silicone Elastomer Kit, Dow Corning Corp., Midland, MI, USA) which provides a reproducible and optically and acoustically transparent device. Using the software CleWin 4.0 (WieWeb software, Hengelo, Netherlands), two types of microchannel designs were created. Straight channels (200, 400 or 600  $\mu\text{m}$  in width and 72  $\mu\text{m}$  in height) and a highly branched channel (ranging from 25 to 600  $\mu\text{m}$  in width and 66  $\mu\text{m}$  in height). The branched microchannels can provide information on bubble behavior at branching points. Schematics of the microchannels are provided in Figure 1.

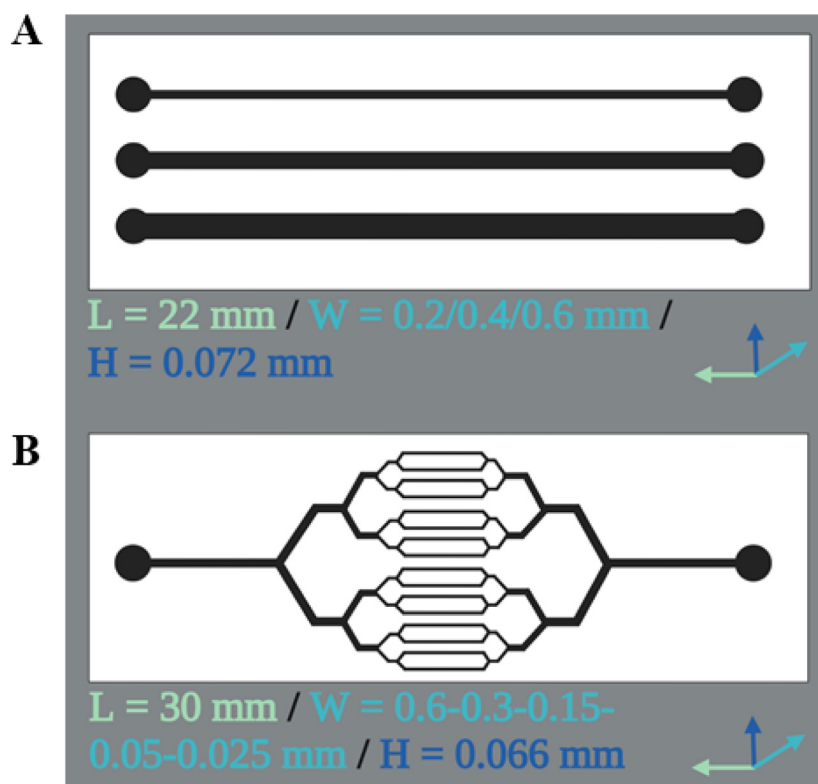


Fig. 1. Design and dimensions of the microchannels used. The microfluidic channels were either straight (A) or branched (B).

The PDMS microchannels were fabricated by a standard soft-lithography and mold-replica process (Alrifaiy *et al.* 2012). An approximately 70- $\mu\text{m}$ -thick layer of negative m-DWL 100 (Micro Resist Technology GmbH, Berlin, Germany) photoresist was spin-coated on top of a silicon wafer (Siegert Wafer, Aachen, Germany). Soft bake was performed to evaporate excess solvents and prepare the resist for UV exposure. UV exposure was carried out by uploading the mask file to the software of a MLA150 Maskless Aligner (Heidelberg Instruments Mikrotechnik GmbH, Heidelberg, Germany), with exposure at a wavelength of 405 nm and dose of 1200 mJ/m<sup>2</sup>. A post-exposure bake was performed, and uncrosslinked mr-DWL 100 was removed using mr-Dev 600 Developer solution (Micro Resist Technology GmbH) followed by a hard bake. The pattern was transferred as a solid mold on the wafer. The mixture of PDMS pre-polymer and curing agent in the ratio of 10:1 was poured onto the photoresist patterned silicon wafer and cured at 65°C for 3 h. A 1-mm blunt needle puncher was used to create inlets and outlets. Subsequently, the PDMS channels were peeled from the molds and bonded via oxygen plasma treatment (150 W, 5 min) (Su 2018) to a layer of PDMS, which was dispersed on top of a Mylar sheet. Final devices consisted of patterned PDMS bonded to PDMS on top of a Mylar sheet, mounted on a custom frame. Twenty-three-gauge fitted stainless-steel fluidic couplers were used to connect Tygon tubing to the PDMS device (Darwin Microfluidics, Paris, France).

#### *Optical–acoustical setup*

Ultrafast microscopy imaging was used to visualize the ultrasound-induced ACT<sup>®</sup> bubble behavioral dynamics using the ultrafast microscopy system at University of Pittsburgh Medical Center (UPMC-Cam) (Chen *et al.* 2013). The system can record up to 25 million frames per second (Mfps). We recorded the activation step, visualizing the transition from ACT<sup>®</sup> microclusters to ACT<sup>®</sup> bubbles, as well as the enhancement step, visualizing the oscillation behavior of ACT<sup>®</sup> bubbles.

The optical–acoustical set up was similar to those in previous studies (Helfield *et al.* 2016a, 2016b). Briefly, a water tank was constructed to house both a single-element transducer at an angle of 45° from below and a white light illumination fiberoptic (Fig. 2). The tank was filled with de-ionized water and placed under a 10 × (UMPlanFL N 10 × /0.30 W, Olympus) or 40 × water immersion objective lens (LUMPLFL, 40 × /0.80 W, Olympus), coupled to a 2 × magnifier and to the UPMC-Cam (Chen *et al.* 2013). By use of a 40 × objective, high-speed recordings were obtained between 5 and 10 Mfps, capturing bubble responses

during 4- to 8-cycle ultrasound pulse excitations. A 10 × objective and “regular” video recording (15 fps) were used to quantify the number of ACT<sup>®</sup> bubbles generated by one single pulse of 8 cycles of ultrasound using a charge-coupled device (CCD) camera.

#### *Experimental protocol*

Microscopy of ultrasound-stimulated transition from ACT<sup>®</sup> microclusters to ACT<sup>®</sup> bubble and ACT<sup>®</sup> bubble behavioral dynamics was recorded as described previously (Chen *et al.* 2013). Briefly, a custom-made water tank held at 35°C housed any of three single-element transducers employed for this study ( $f = 0.5$  MHz, focal distance 42.4 mm, Model A301 S-SU-F1.65-PTF;  $f = 1$  MHz, focal distance 41.4 mm, Model A302 S-SU-F1.63-PTF;  $f = 2.25$  MHz, focal distance 25.4 mm, Model C323-SU-F1.0-PTF; Olympus NDT, Waltham, MA, USA) at an angle of 45° from below along with a port to house the light guide used to deliver constant (15-fps recordings for 10–20 s) and flash lamp illumination (107-fps recordings of 128 frames) (Fig. 2). Optical–acoustical co-alignment was performed with a pulse–echo approach described by Chen *et al.* (2013). The ultrasound transducer was driven by an arbitrary function generator (AFG3252, Tektronix, Beaverton, OR, USA) and a gated power amplifier (Model 250A250AM8, Amplifier Research, Souderton, PA, USA). The ultrasound delivery system was calibrated in a separate water tank with a hydrophone (HGL-0200, Onda, Sunnyvale, CA, USA).

The efficiency of the activation step of microclusters was recorded with a standard CCD camera. The microcluster suspension was prepared per the manufacturer's instructions, diluted 120-fold in undersaturated saline at room temperature and injected into the microchannels. Experiments were performed with no fluid flow. The activation step was recorded during insonication of the microcluster suspension using a single 8-cycle ultrasound pulse at 0.5, 1 or 2 MHz. The transmit pulses were sent at a peak negative pressure from 0.1 to 0.6, 0.2 to 1.0 and 0.1 to 0.8 MPa for 0.5, 1 and 2 MHz, respectively. These exposure parameters are in the same range as used in our previous pre-clinical studies (van Wamel *et al.* 2016b; Aslund *et al.* 2017).

The enhancement step was recorded with the UPMC camera. First, ACT<sup>®</sup> bubbles were activated in the microchannels using an 8-cycle ultrasound pulse at 1 MHz and 1 MPa. For the enhancement step, the ACT<sup>®</sup> bubbles were insonicated with a single 4-cycle ultrasound pulse at 0.5 MHz at pressures ranging from 0.063 to 0.60 MPa or an 8-cycle ultrasound pulse at 1 MHz at pressures from 0.2 to 1.0 MPa. Both frequencies were generated with the same transducer.

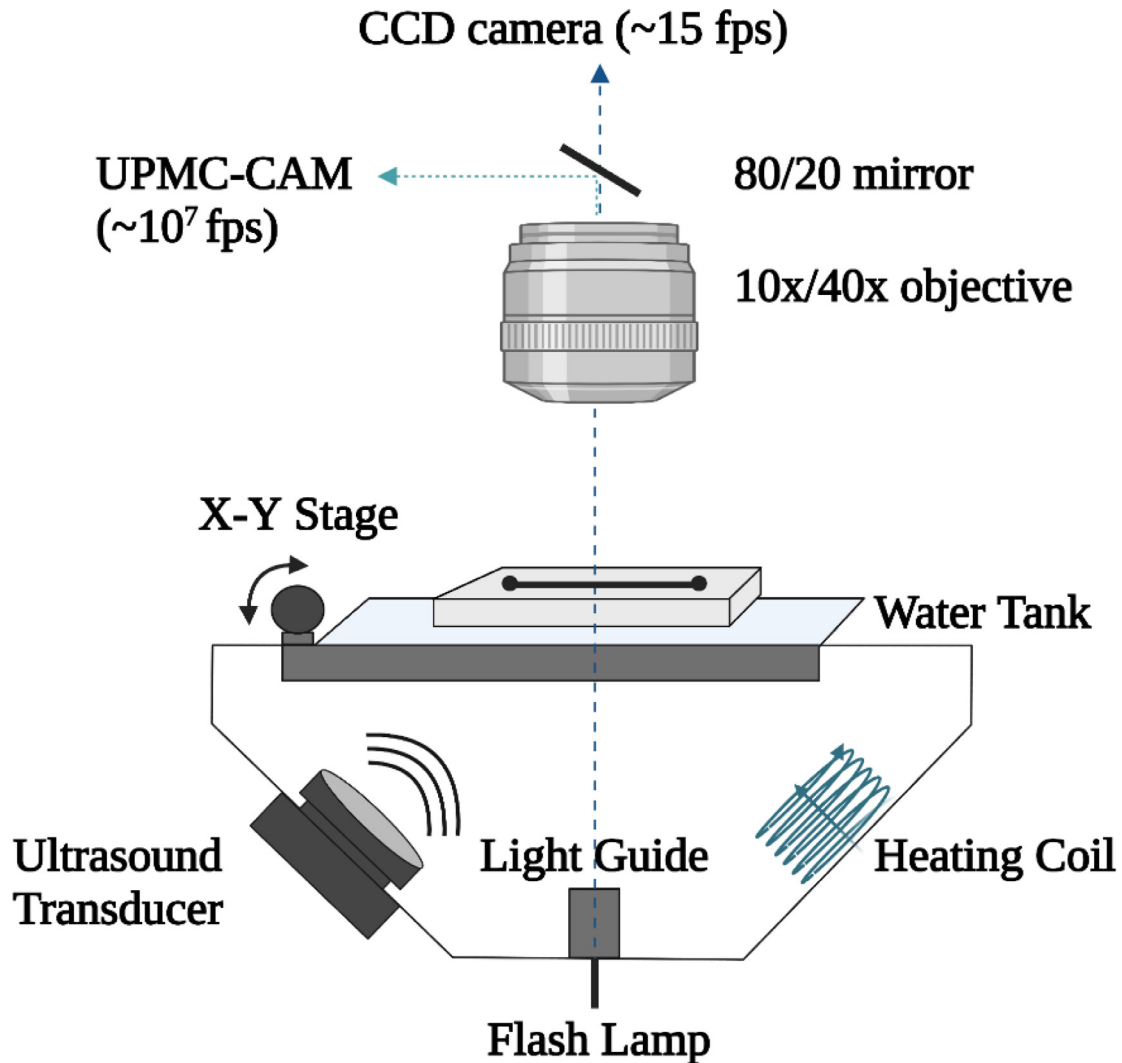


Fig. 2. Schematic of the experimental optical–acoustical setup. CCD = charge-coupled device; UPMC-CAM = ultrafast microscopy system developed at the University of Pittsburgh Medical Center.

#### Analysis of the recorded videos and oscillations

ACT bubble dynamics were extracted from the 128 images recorded at 5–10 Mfps. The diameter–frame number curves of individual bubbles were measured using image analysis software (MIPAR, Columbus, OH, USA). The border of the bubble of interest was annotated in the first frame of the recording and used to radially resample the bubble and its direct surrounding. The resulting image was used as an input to the algorithm to find the optimal path along the contour of the bubble, and the average bubble diameter was determined. This was then used to repeat the above procedure for the next frame. After running through all frames, the diameter–time curve of the bubble was obtained. Spatial calibration was obtained by imaging a high-resolution calibration target (1951 USAF Glass Slide Resolution Targets, Edmund Optics Inc., Barrington, NJ, USA) with identical optical settings (Chen et al.

2013). Temporal information (the actual recording speed) for each video was obtained from onboard information generated from multiple photodiode detectors and stored with the video files. The maximum and minimum radii of each oscillating ACT<sup>®</sup> bubble were determined.

*Simulation of bubble oscillations.* To simulate the radial oscillation of an unshelled gas bubble, the modified Rayleigh–Plesset equation was used (Rayleigh 1917; Plesset 1949):

$$\begin{aligned} & \rho \left( R\ddot{R} + \frac{3}{2}\dot{R}^2 \right) \\ &= \left( p_0 + \frac{2\sigma}{R_0} \right) \left( \frac{R_0}{R} \right)^{3\kappa} \left( 1 - 3\kappa \frac{\dot{R}}{c} \right) - \frac{2\sigma}{R} - 4\mu \frac{\dot{R}}{R} \\ & \quad - \delta_t \omega \rho R \dot{R} - p_0 - p_{ac} \end{aligned} \quad (1)$$

where  $R$  is the instantaneous radius of the bubble,  $R_0$  is the equilibrium bubble radius,  $\rho$  is the density of the surrounding liquid,  $p_0$  is the hydrostatic pressure,  $\sigma$  is the surface tension of the liquid–gas interface,  $\kappa$  is the polytropic exponent of the gas,  $\mu$  is the viscosity of the liquid,  $\delta_t$  is a dimensionless coefficient for thermal damping,  $\omega$  is the angular frequency of the acoustic pressure,  $p_{ac}$  is the driving pressure, where the overdots denote differentiation with time.

The phase transition of a microdroplet into an ACT<sup>®</sup> bubble generates a bubble not encapsulated in a shell, as the resultant surface area of the bubble is much larger than the surface area of the microcluster, and therefore there are not sufficient lipids to cover the large bubble surface. The shell material of the Sonazoid bubble may partly be in the solution and/or partly along regions of the gas–liquid interface. Equation (1), therefore, does not contain any shell terms which are necessary when simulating the response from commercially available microbubbles such as SonoVue or Sonazoid. However, a term accounting for thermal damping is included. Thermal damping is associated with heating and cooling of the gas during compression and expansion, respectively, and resulting heat transfer between the gas and the surrounding liquid. It is challenging to include thermal damping into the non-linear Rayleigh–Plesset equation in a stringent way. In the current work, this was done in a manner similar to that used by Eatock *et al.* (1985), and the dimensionless coefficient for thermal damping was estimated based on the work by Medwin (1977):

$$\delta_t = \left(\frac{d}{b}\right) \left(\frac{f_r}{f}\right)^2 \quad (2)$$

Here,  $f_r$  is the resonance frequency and  $f$  is the driving frequency. For bubbles with radii around 10  $\mu\text{m}$ , such as ACT<sup>®</sup> bubbles, thermal damping is typically the dominant form of energy loss, and the use of an augmented viscosity is less appealing. For commercial microbubbles with typical radii of 1–2  $\mu\text{m}$ , thermal damping is of the same order of magnitude as viscous damping, and it is therefore common to use an augmented viscosity to account for thermal damping instead (Van Der Meer *et al.* 2007).

Because of buoyancy, the bubbles will be situated close to the top of the microchannel during optical imaging. Equation (1) is valid for a bubble oscillating in free space without any effects from nearby boundaries. Cavitation bubble behavior has been analyzed near boundaries with different elasticities, and it was found that gels with a Young's modulus similar to that of PDMS, typically 1 MPa (Johnston *et al.* 2014), resemble the case of a rigid boundary (Brujan *et al.* 2000). The walls of the

microchannel were therefore considered to be rigid boundaries where the normal component of the fluid velocity and the normal gradient of the pressure must be zero. To account for the effect of such a rigid boundary, a common approach is to introduce an imaginary image bubble oscillating in phase with the real bubble that is placed symmetrically with respect to the boundary plane (the top wall of the microchannel). Substituting the terms on the right-hand side of eqn (1) with  $P$ , this equation can then be written as

$$\rho \left( R\ddot{R} + \frac{3}{2}\dot{R}^2 \right) = P - \rho \left( R\ddot{R} + 2\dot{R}^2 \right) \frac{R}{2d} \quad (3)$$

which also was suggested by Doinikov *et al.* (2009). Here,  $d$  is the distance between the center of the bubble and the rigid boundary, and  $2d$  is hence the distance between the centers of the real and imaginary bubbles.

The viscous shear stress exerted on a nearby solid boundary by an oscillating bubble was estimated as described by Helfield *et al.* (2016b):

$$\tau = \mu \frac{\partial V}{\partial Z} \approx 2(\mu\rho)^{1/2} (\pi f)^{3/2} \varepsilon R_0 \quad (4)$$

Here,  $f$  is the ultrasound frequency, and  $\varepsilon$  is the relative radial expansion,  $\varepsilon = (R_{\max} - R_0)/R_0$ .

## RESULTS AND DISCUSSION

### *Activation step: From microclusters to ACT<sup>®</sup> bubbles*

#### *High-speed recording of activation of ACT<sup>®</sup> bubble*

The PS101 solution contains approximately twice as many microbubbles as microdroplets, and because of this excess of microbubbles, the microcluster will typically contain a single microdroplet surrounded by two or more microbubbles (Sontum *et al.* 2015). The formation of ACT<sup>®</sup> bubbles were recorded using high-speed imaging, and from such recordings (Video S1, online only), the changes in bubble radius as a function of time during the 17- $\mu\text{s}$  recording are visible (Fig. 3). The high-speed videos indicate how the microbubble–microdroplet, forming a microcluster, fused and the gas in the microbubble acted as a vaporization seed for the oil in the microdroplet, and a precursor ACT<sup>®</sup> bubble was formed. This precursor bubble subsequently grew in size as a result of inward gas diffusion from the surrounding medium and became a large ACT<sup>®</sup> bubble. The transition of the microclusters into precursor bubbles is a novel observation, whereas the subsequent growth into large ACT<sup>®</sup> bubbles has been described previously (Sontum *et al.* 2015; Kotopoulos *et al.* 2017). The formation of the large ACT<sup>®</sup> bubble is in accordance with observations of bubbles lodging in capillaries in tumor tissue in mice (van Wamel *et al.* 2016a).

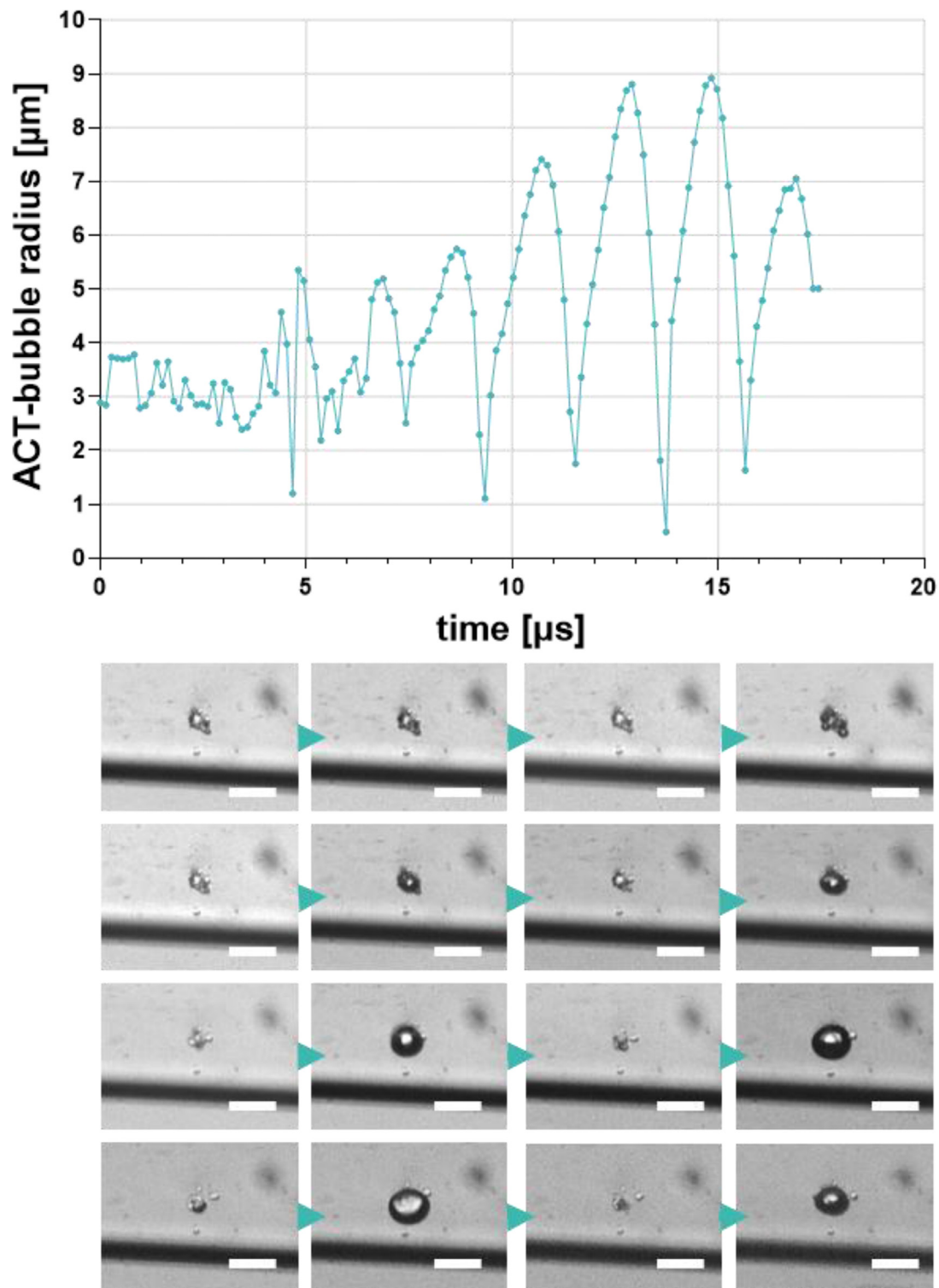


Fig. 3. A microdroplet–microbubble microcluster was recorded while insonated with one burst of eight cycles of ultrasound with a frequency of 0.5 MHz at 0.30 MPa. Changes in bubble radius during insonication for 17  $\mu\text{s}$  resulted in a growing bubble. Sixteen frames indicating the response at maximum positive and negative pressures were selected. Imaging was performed at 7.28 Mfps and 40 $\times$  magnification. Bar = 20  $\mu\text{m}$ . ACT = Acoustic Cluster Therapy.

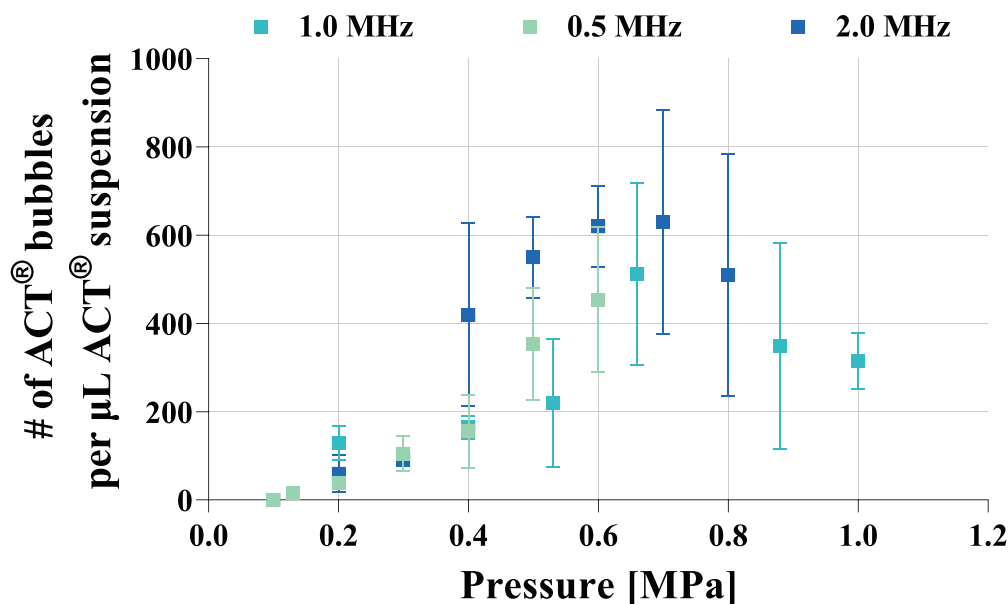


Fig. 4. Number of ACT<sup>®</sup> bubbles generated in 140 individual recordings of microclusters insonified with different frequencies at different pressures per microliter of microcluster suspension. The mean is based on two to seven measurements. Bars indicate standard deviations. ACT = Acoustic Cluster Therapy.

#### *Optimal frequency and pressures for activation.*

The efficiency in activation of the microclusters was compared for three different frequencies, 0.5, 1.0 and 2.0 MHz, and pressures in the range 0.1–1.0 MPa (Fig. 4). For all frequencies, a pressure >0.1 MPa was needed to create ACT<sup>®</sup> bubbles. This threshold effect was seen for all frequencies and is consistent with measurements using a sonometry system (Healey *et al.* 2016). There was a large variation in the number of activated bubbles in the field of view per video acquisition as indicated by the large standard deviations. Because of the large standard deviation, no statistical differences were found above the threshold, but some trends in the number of activated ACT<sup>®</sup> bubbles as a function of acoustic pressures were observed.

The maximum number of ACT<sup>®</sup> bubbles was seen for 2 MHz when applying 0.6–0.7 MPa, which is consistent with the resonance frequency of Sonazoid, as the activation depends on Sonazoid to oscillate and initiate fusion with the microdroplet. Sonazoid has an average diameter of 2.6  $\mu\text{m}$ ; thus, the resonance frequency is estimated at approximately 2.3 MHz (Kooiman *et al.* 2014). Increasing the pressure further when applying an ultrasound frequency of 1.0 MHz reduced the number of activated bubbles. The reduction might have occurred because this high pressure destroys the Sonazoid microbubbles, fragmenting them rather than have them oscillating and fusing them with the microdroplets, or because non-linear oscillations limit the fusion capabilities to the microdroplet, thereby preventing activation. In line with these explanations,

destruction of contrast agent microbubbles has been reported at such high pressures (Postema *et al.* 2004; Bouakaz *et al.* 2005; Yeh and Su 2008), and cavitation is reported within microseconds (Kudo *et al.* 2002).

A maximum of 630 ACT<sup>®</sup> bubbles/ $\mu\text{L}$  microcluster suspension was generated using only one burst of 8 cycles of 2 MHz at a pressure of 0.7 MPa. The microcluster suspension consisted of  $1.1 \times 10^6$  microbubbles/ $\mu\text{L}$  and  $3 \times 10^5$  microdroplets/ $\mu\text{L}$ , which translated into  $4.7 \times 10^4$  clusters/ $\mu\text{L}$  (Certificate of Analysis, EXACT Therapeutics). Thus, in our experiments, a maximum of 1.34% of the microclusters were activated within the image frame with a single ultrasound pulse of 4  $\mu\text{s}$ . This is rather efficient in such a short time, and increasing the number of pulses will increase the number of activated bubbles.

*Sizes and shapes of activated ACT<sup>®</sup> bubbles.* The diameters of the spherical activated ACT<sup>®</sup> bubbles ranged from 5 to 50  $\mu\text{m}$  (Fig. 5), and most of the bubbles in the microchannels with widths >25  $\mu\text{m}$  had diameters of 15–25  $\mu\text{m}$ , as previously reported (Sontum *et al.* 2015; Healey *et al.* 2016). No significant difference in ACT<sup>®</sup> bubble size was observed for the different activation frequencies used. For 25- $\mu\text{m}$ -wide channels, the average bubble diameter was 16  $\mu\text{m}$ . Increasing the size of the microchannel in the range 50–600  $\mu\text{m}$  provided more space for the ACT<sup>®</sup> bubble, but did not increase the diameter of the activated bubble, indicating a maximum bubble size. The size of the ACT<sup>®</sup> bubble depends on the diffusion of gas from the

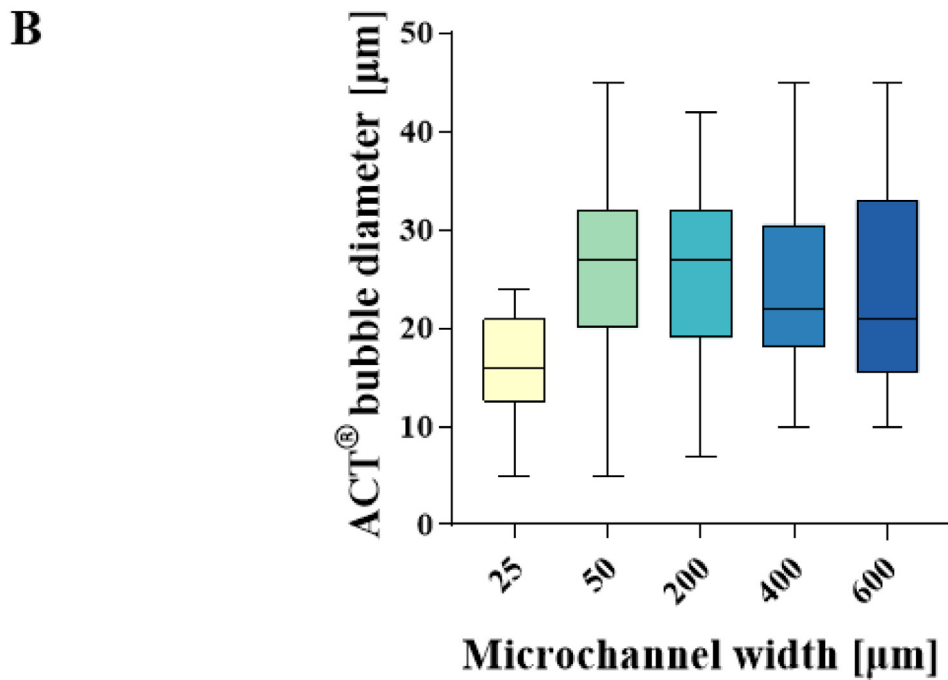
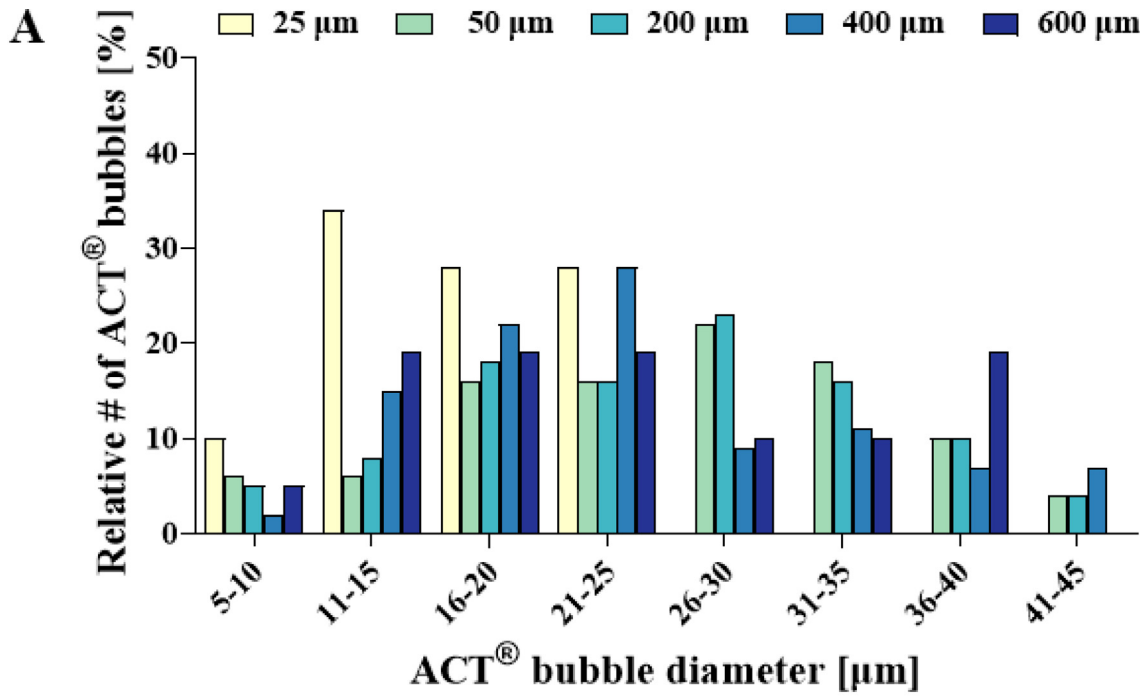


Fig. 5. (A) Relative number of ACT® bubbles as a function of ACT® bubble diameter in different sizes of microchannels. (B) ACT® bubble diameter obtained in microchannels of increasing width. ACT = Acoustic Cluster Therapy.

surrounding medium into the bubble, and in the case of microchannels 25  $\mu\text{m}$  wide, the diffusion of gas might be limited. In accordance with our observations, ACT<sup>®</sup> bubbles in phosphate-buffered saline have been reported to have diameters up to 40–50  $\mu\text{m}$ , but in serum albumin, the ACT<sup>®</sup> bubbles were smaller and diameters up to 20  $\mu\text{m}$  were measured. The smaller sizes were reported to be caused by the breaking up of larger clusters in serum albumin (Healey *et al.* 2016).

Five different shapes of ACT<sup>®</sup> bubbles were observed (Fig. 6). In two dimensions they appeared as round circles either free floating or probably floating up and in contact with the top wall of the microchannel (Fig. 6a) or adhering to the microchannel side wall (Fig. 6b). The bubbles also formed a half-bubble (Fig. 6c), were cigar shaped (Fig. 6d) and were square shaped (Fig. 6a). The circular bubbles were observed in all microchannels independent of the dimensions of the channel, indicating that when the space around the microcluster was “unlimited,” spherical bubbles were formed. For channels  $\leq 50$   $\mu\text{m}$ , the ACT<sup>®</sup> bubbles could stick to one side of the channel, forming a half-bubble. In smaller channels 25  $\mu\text{m}$  wide, the bubbles predominantly formed round, square or cigar-shaped bubbles with a curved surface across the channel. These bubbles could cover more than tens of micrometers along the microchannel wall. Although the microchannel is rectangular and rather rigid, the elongated shape of the bubbles indicates that ACT<sup>®</sup> bubbles could also cover a larger segment of the capillary wall in elastic capillaries (tens to hundreds of micrometers depending on the capillary diameter) as seen in mesentery microvasculature (Sontum *et al.* 2015). Sontum and colleagues observed, using intravital microscopy, that activated ACT<sup>®</sup> bubbles had an ellipsoidal shape, blocked the capillary and lodged in the rat mesentery microvasculature for

5–10 min. On comparison of the echo contrast signals from ACT<sup>®</sup> bubbles and the commercial Sonazoid, the echoes from ACT<sup>®</sup> bubbles were stationary for 2–5 min and disappeared completely after 15 min, whereas the signal from Sonazoid microbubbles disappeared from the vasculature within 1–2 min (van Wamel *et al.* 2016a). The long resistance time of ACT<sup>®</sup> bubbles makes ACT<sup>®</sup> bubbles a valuable contrast agent that can be used to predict the therapeutic outcome (Bush *et al.* 2020).

Microbubbles that remain in the vasculature for long time are an advantage when used clinically for ultrasound-mediated drug delivery, to avoid repeated injections or continued infusions of microbubbles. Thus, there are various approaches making novel microbubbles designed for drug delivery having long circulation times (Abou-Saleh *et al.* 2016; Ingram *et al.* 2020).

*Coalescing and dissolving of ACT<sup>®</sup> bubbles.* The activated large ACT<sup>®</sup> bubbles might undergo coalescence generating even larger bubbles, and some bubbles might be dissolved because of gas diffusion, as illustrated in Video S2 (online only). Four selected frames from the video are provided in Figure 7. Four seconds after the ultrasound is turned on, two ACT<sup>®</sup> bubbles close to each other coalesce probably because of secondary Bjerknes (1906) forces. The figures also reveal one activated bubble decreasing in size and dissolving over time.

#### *Enhancement step: ACT<sup>®</sup> bubble behavior*

##### *Spherical activated bubbles and oscillations.*

High-speed recordings of ACT<sup>®</sup> bubbles between 5 and 50  $\mu\text{m}$  and insonified with one burst of 4 cycles at 0.5 MHz and pressures between 0 and 0.60 MPa ( $n = 80$

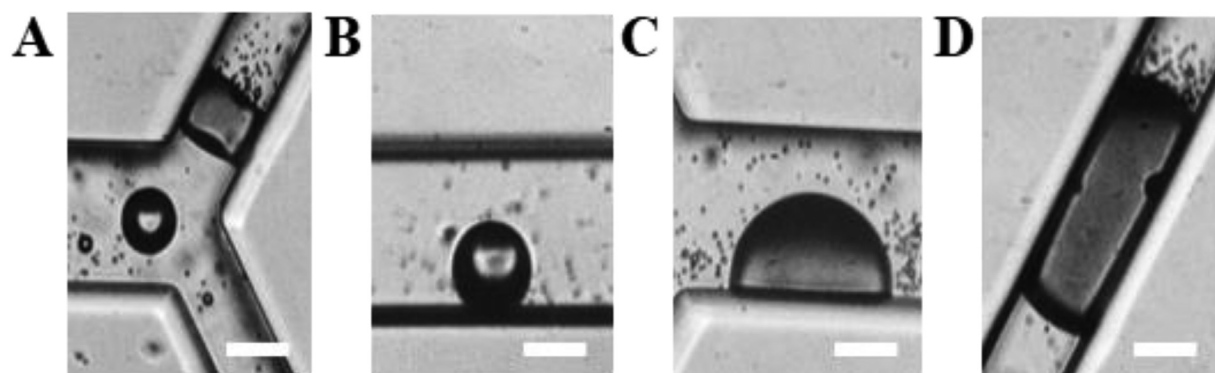


Fig. 6. Different shapes of ACT<sup>®</sup> bubbles observed. (A) A circular bubble probably in contact with the top wall and (B) a circular bubble adhering to the side wall were observed in all channel sizes. (C) A half-circle-shaped bubble was seen in channels 200  $\mu\text{m}$  wide and narrower. (D) Cigar-shaped and (A) square adhering bubbles were seen only in 25- $\mu\text{m}$  channels. In addition to the activated ACT<sup>®</sup> bubbles, non-activated microclusters and microbubbles were seen. Bar = 25  $\mu\text{m}$ . ACT = Acoustic Cluster Therapy.

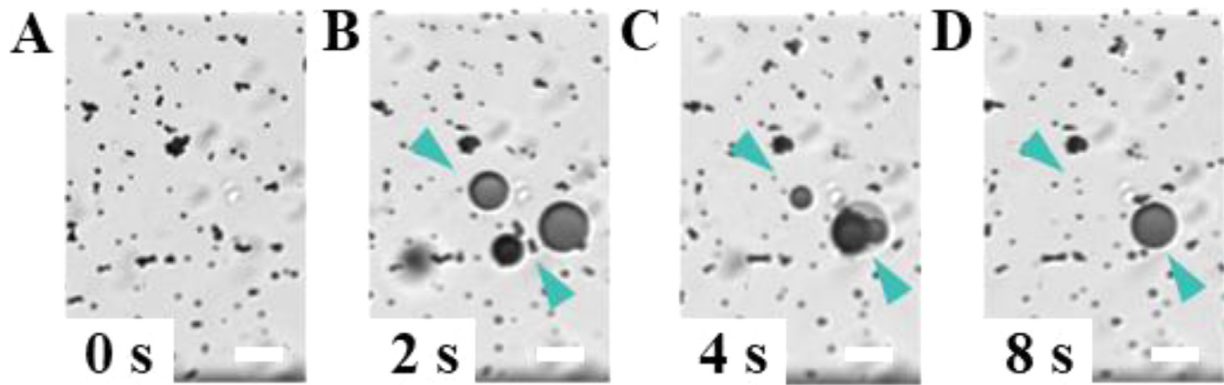


Fig. 7. Four selected frames of creation of ACT<sup>®</sup> bubbles in a 200- $\mu\text{m}$  channel. (A) Frame just before ultrasound,  $t = 0$ . (B) Frame 2 s ( $t = 2$  s) after the burst of 8 cycles of ultrasound with a frequency of 2 MHz at 400 kPa. Marked by *arrows* are three ACT<sup>®</sup> bubbles, one of which is dissolving and two are coalescing into one. (C, D) Frames at  $t = 4$  s and  $t = 8$  s, respectively. Bar = 25  $\mu\text{m}$ . ACT = Acoustic Cluster Therapy.

ACT<sup>®</sup> bubbles) or at 1 MHz and pressures between 0 and 1.0 MPa ( $n = 40$  ACT<sup>®</sup> bubbles) were analyzed. A representative video can be seen in Video S3 (online only). Maximum and minimum radii were determined for each ACT<sup>®</sup> bubble, and the maximum displacement ( $R_{\text{max}} - R_0$ ) is plotted against the initial ACT<sup>®</sup> bubble radius in Figure 8.

Exposure to 0.5 MHz resulted in larger amplitudes of oscillations than 1-MHz exposure. Bubbles with an initial radius of 5  $\mu\text{m}$  had the largest increase in radius. This is in accordance with the expected resonance frequency, which is approximately 0.6 MHz for bubbles with a radius of 5  $\mu\text{m}$  (Kooiman et al. 2014). The change in bubble radius increased with increasing pressure. For 0.5 MHz, the average radius increase, that is, displacement, was 1.3, 2.4, 2.7 and

2.7  $\mu\text{m}$  for driving pressures of 127, 190, 254 and 500 kPa, respectively. For 1 MHz, the average radius increase, that is, displacement, was 0.5, 0.9, 1.5 and 1.7  $\mu\text{m}$  for driving pressures of 200, 400, 500 and 1000 kPa, respectively.

The experimental data for the oscillations of ACT<sup>®</sup> bubbles presented in Video S3 were compared with simulations of radial oscillations using eqn (1) for a free space situation and eqn (3) for a situation when the microbubble is located next to a solid boundary introduced by the top wall of the microchannel. The following parameters were applied in the simulations:  $p_0 = 1.013 \times 10^5$  Pa,  $\rho = 1000$  kg/m<sup>3</sup>,  $\mu = 1 \times 10^{-3}$  Pa·s,  $\sigma = 0.072$  N/m,  $\kappa = 1.1$  and  $\delta_t = 0.11$  and 0.029 for the small and large bubbles, respectively (Medwin 1977). Figure 9A illustrates the drive pulse measured by

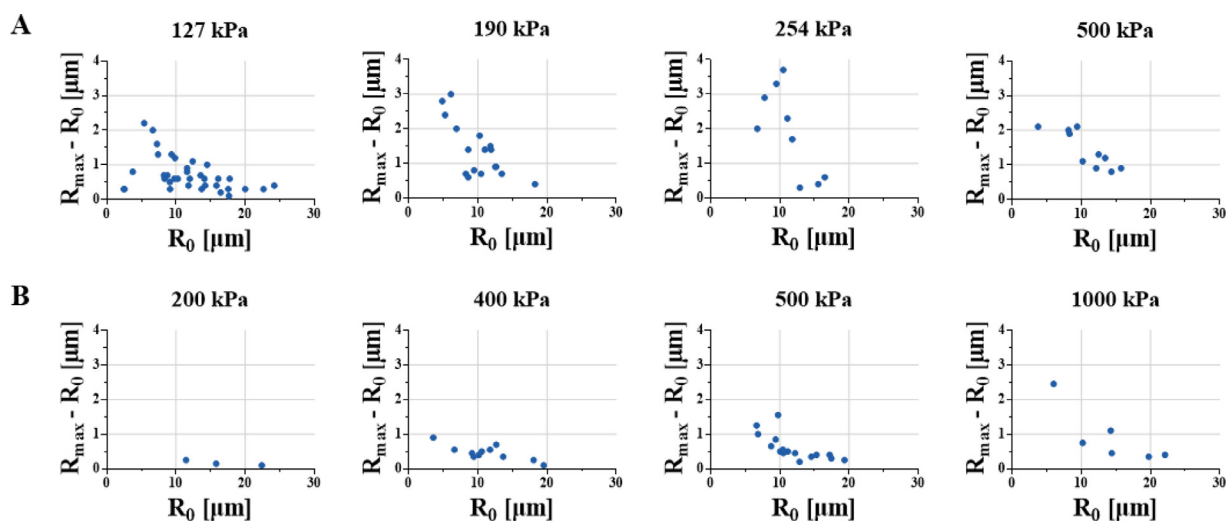


Fig. 8. Maximum displacement ( $R_{\text{max}} - R_0$ ) as a function of initial radius  $R_0$  for individual ACT<sup>®</sup> bubbles. (A) At a driving frequency of 0.5 MHz and driving pressures of 127, 190, 254 and 500 kPa, respectively. (B) At a driving frequency of 1.0 MHz and driving pressures of 200, 400, 500 and 1000 kPa, respectively. ACT = Acoustic Cluster Therapy.

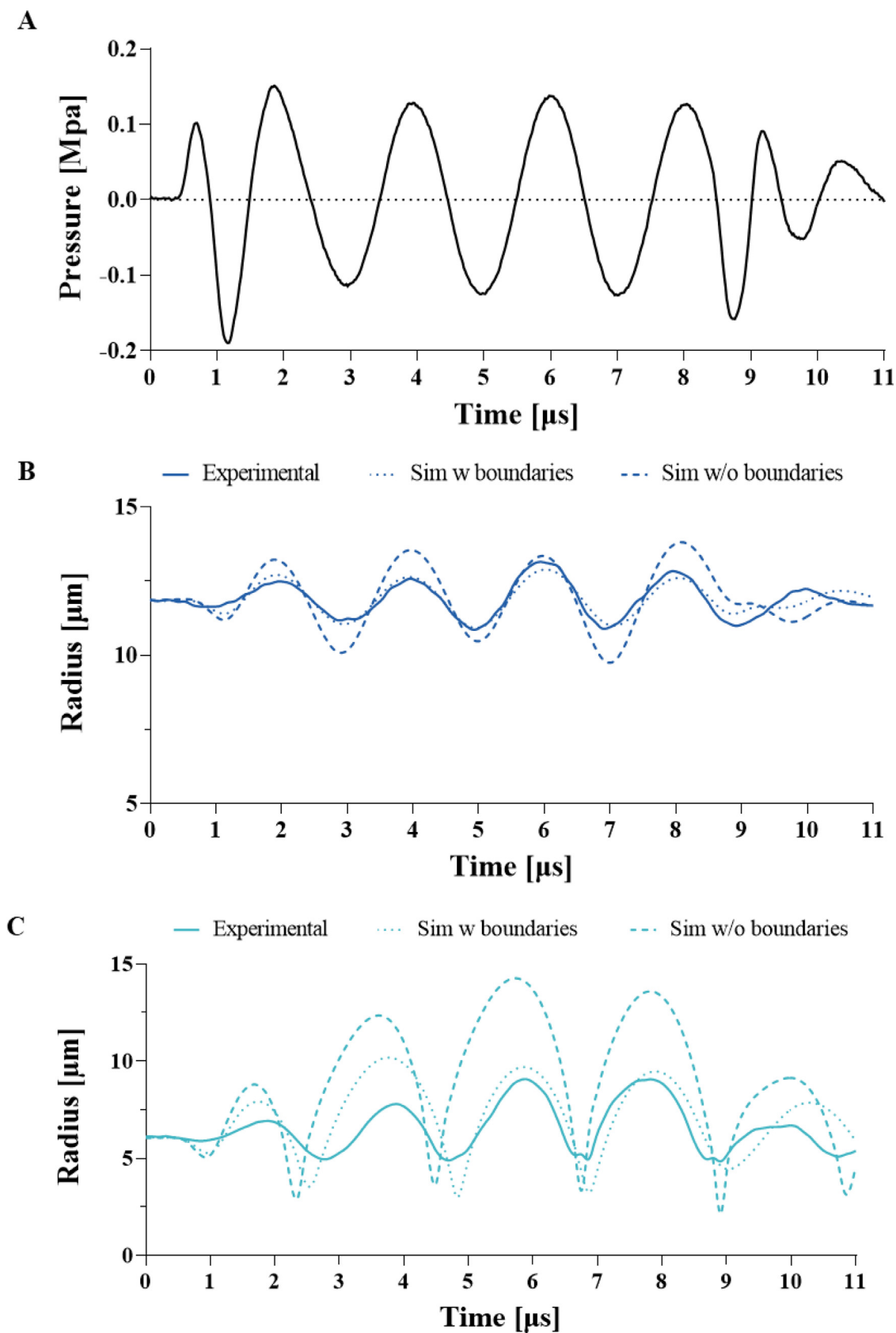
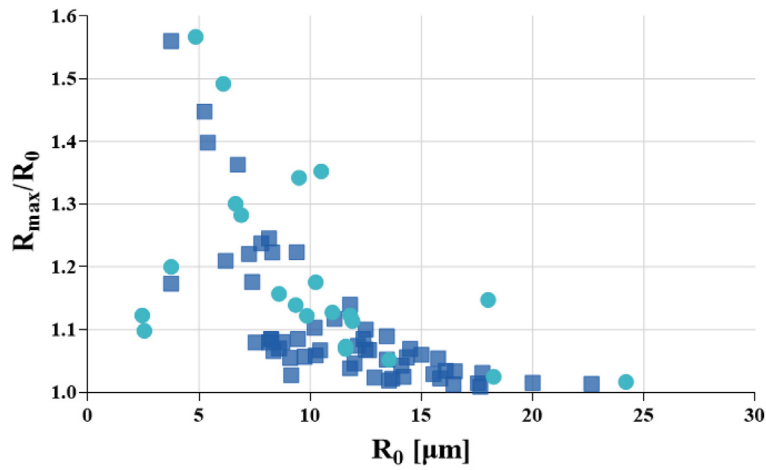
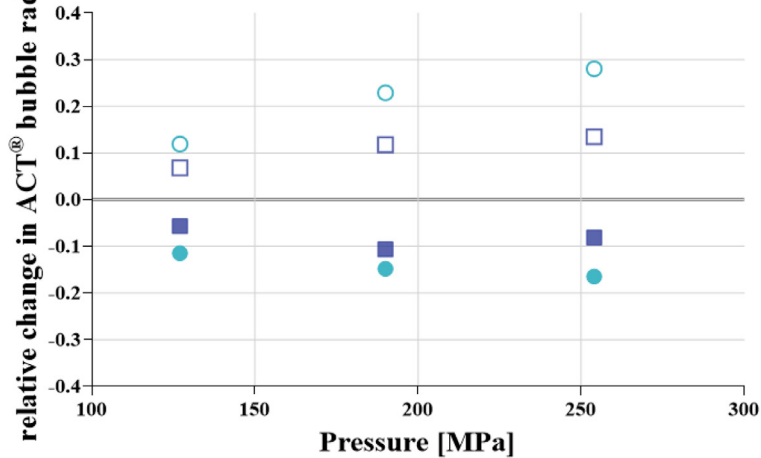


Fig. 9. (A) Measured drive pulse. (B) Radius oscillations for an ACT<sup>®</sup> bubble with an initial radius of 12.0  $\mu\text{m}$ . (C) Radius oscillations for a bubble with an initial radius of 6.1  $\mu\text{m}$ . *Dashed lines* are obtained by placing the bubble next to a rigid boundary. *Dash-dot lines* are obtained using a regular free space situation. ACT = Acoustic Cluster Therapy.

**A** ● ACT<sup>®</sup> bubbles touching one channel wall ■ ACT<sup>®</sup> bubbles touching two channel walls



**B** ● / ○ ACT<sup>®</sup> bubbles touching one channel wall compression / expansion  
 ■ / □ ACT<sup>®</sup> bubbles touching two channel walls compression / expansion



**C** ● ACT<sup>®</sup> bubbles touching one channel wall ■ ACT<sup>®</sup> bubbles touching two channel walls

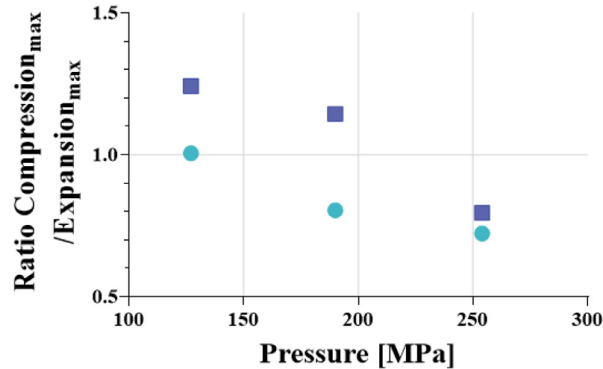


Fig. 10. Comparison of oscillations at 0.5 MHz of ACT bubbles when touching the top wall versus two walls touching. (A) Ratio of maximum bubble radius and initial bubble radius as a function of the initial radius. All microbubbles exposed to driving pressures between 63 and 500 kPa are included. (B) Comparison of relative change in radius as function of pressure. (C) Ratio maximum compression ( $R_0 - R_{min}$ )/maximum expansion ( $R_{max} - R_0$ ) as a function of pressure. ACT = Acoustic Cluster Therapy.

a hydrophone in a water tank. A transducer with a center frequency of 1 MHz was driven by a four-cycle excitation pulse of 0.5 MHz, and the resulting acoustic pulse is therefore somewhat distorted.

In Figure 9B and 9C, the vibration amplitudes for two different ACT<sup>®</sup> bubbles with initial radii of 12.0 and 6.1 mm, respectively, are illustrated. The *solid lines* represent optical measurements, the *dash-dotted lines* are obtained from simulations in a free space situation and the *dashed lines* are from simulations with a rigid boundary placed next to the bubbles to emulate bubbles oscillating near the top wall of the microchannel. The presence of a rigid boundary significantly dampens the vibration amplitude in the simulations, and it can be seen that simulation and optical measurements correlate much better when using this rigid boundary condition. This indicates that the ACT<sup>®</sup> bubbles probably floated to the top of the microchannel because of buoyancy and encountered the ceiling of the channel (top wall). The agreement between measurement and simulation is especially good for the larger bubble (radius = 12 μm). Not accounting for the rigid boundary condition seems to have a larger impact on the oscillations for the smaller bubble than the larger bubble, which is consistent with larger-amplitude oscillations for the 6-μm bubble compared with the 12-μm bubble.

The larger-amplitude oscillations for the 6-μm bubble compared with the 12-μm bubble are probably due to its resonance frequency being closer to the driving frequency at 0.5 MHz. Larger oscillations will also result in a stronger interaction with the physical boundaries of the microchannel. A main limitation of the simulation model is that spherical bubble oscillations are assumed. This assumption will be less valid with a stronger interaction between the physical boundaries and the bubble. A more pronounced deviation from spherical oscillations may explain the larger discrepancy between experimental observations and simulation results for the small bubble compared with the large bubble.

The observed spherical bubbles were either (i) free floating or most likely in contact with the top wall of the microchannel or (ii) touching the top and side walls of the microchannel (Fig. 6A, 6B). In a blood vessel, the ACT<sup>®</sup> bubble will be in contact with the vessel wall or block the vessel, as illustrated in rat mesentery microvessels (Sontum *et al.* 2015). Thus, understanding the impact of adhering to a wall is of interest, and the oscillations of an “upward floating” bubble and an “upward floating” bubble also adhering to the side wall were compared. Figure 10A illustrates the relative changes in maximal radius as a function of initial radius for all pressures applied at 0.5 MHz. The “upward floating” and two wall-touching bubbles seemed to have similar bubble response, when microbubbles exposed to all driving

pressures are pooled together. However, by presenting the relative extension  $(R_{\max} - R_0)/R_0$  and compression  $(R_{\min} - R_0)/R_0$  as a function of acoustic pressure applied (Fig. 10B), it can be seen that for the bubble probably in contact with the top wall, there were approximately twice as much relative change as a function of acoustic pressure compared with the bubble also adhering to the microchannel side wall. The bubble radius increased with increasing applied pressure. Interestingly, on comparing the compression and the expansion (Fig. 10C), the bubbles also adhering to the channel side wall exhibited relative larger compression than expansion for the two lowest pressures applied, whereas the “upward floating” bubbles exhibited larger expansion than compression for the two highest pressures.

The maximum percentage change in radius during expansion is approximately 20%–25% for “upward floating” bubbles and 10%–15% for bubbles also adhering to the side wall (Fig. 10B). The percentage is less than for the regular ultrasound contrast microbubbles such as Sonazoid and SonoVue (Helfield *et al.* 2016b) as the initial radius of the ACT<sup>®</sup> bubble is large. In absolute increase in radius, the change is similar: both the ACT<sup>®</sup> bubble and Sonazoid or SonoVue increase approximately 1–2 μm in radius.

Assuming that the bubble oscillations observed in the rigid microchannels are not much different from oscillations in elastic and probably smaller capillaries, the rather modest change in ACT<sup>®</sup> bubble radius seems to be sufficient for substantial improved therapeutic outcome for tumors growing in mice treated with various drugs in combination with ACT<sup>®</sup> (Van Wamel *et al.* 2016a, 2016b; Kotopoulos *et al.* 2017; Bush *et al.* 2020). The promising therapeutic response of ACT<sup>®</sup> in mice is probably due to the large ACT<sup>®</sup> bubble volume. The volume of the ACT<sup>®</sup> bubbles is 100–600 times larger than the volume of regular contrast agent bubbles. The elongated shape of the bubbles indicates that the ACT<sup>®</sup> bubbles cover a larger segment of the vessel wall than smaller commercial contrast agents, which will contribute to increased biomechanical effect of the vessel wall and potential improved therapeutic outcome. For conventional ultrasound contrast microbubbles, it is reported that it is important that the vessel wall is in proximity to the oscillating microbubble, that is, within 75% of the maximum microbubble radius, to induce sonoporation *in vitro* and *ex vivo* (Gac *et al.* 2007; Chen *et al.* 2010, 2012; Tzu-Yin *et al.* 2013). Microbubble–endothelium interactions have been studied by high-speed imaging, and have revealed microvessel distention of 2.3 μm and invagination of 0.8 μm (Caskey *et al.* 2007). Changing the vessel diameters can induce mechanical effects beyond the vessel into the extracellular matrix, and the large ACT<sup>®</sup>

bubbles might have a larger impact on the vessel diameters and extracellular matrix than the small microbubbles. Another possible mechanism for ACT-induced improved therapeutic outcome is the occlusion of some capillaries, which might increase the microvascular pressure and thereby induce a transcapillary pressure gradient, which is hardly present in most tumors (Boucher and Jain 1992).

#### *Half-circle and square bubbles and rippling.*

ACT bubbles adhered to the microchannel side wall and had various shapes (Fig. 6), either adhering to one side channel wall or blocking the channels. The half-circle bubbles had a typical diameter of 27–42  $\mu\text{m}$ . One characteristic of the half-circle bubbles was surface rippling, which was not seen for spherical “upward floating” bubbles not adhering to the side wall. Surface rippling observed as surface streaks was seen mainly for larger bubbles with diameters  $>36 \mu\text{m}$  and insonified with one burst of 8 cycles at 1 MHz. Squared bubbles that adhered to both side walls of the microchannel also exhibited surface rippling at both 500 kHz and 1 MHz. Figure 11 provides an example of a half-circle bubble and a square bubble with surface rippling. Square ACT<sup>®</sup> bubbles can be seen in Video S4 (online only). Surface rippling is an interesting phenomenon, but probably not relevant in drug delivery as this effect is probably caused by the stiff channel wall.

*Jetting.* For ACT<sup>®</sup> bubbles adhering to the side channel wall or forming half-circle bubbles, that is, experiencing asymmetric boundary conditions, jetting was observed (Video S5, online only). For bubbles blocking the channel, jetting was never observed. Video S5 illustrates an ACT<sup>®</sup> bubble near the side channel wall. On insonation, it starts oscillating. The boundary caused asymmetrical bubble oscillations and led ultimately to the collapse of the bubble, which caused the formation of a high-speed liquid jet. A liquid jet can be seen to be threading through the bubble. Jetting behavior

is described by other groups and reported potentially to puncture the vessel wall (Postema et al. 2004; Wang et al. 2019). Jetting will probably not be an important phenomenon for ACT-enhanced drug efficacy; as in our previous *in vivo* studies (van Wamel et al. 2016b; Bush et al. 2020), low pressures were used, and bubbles will be in contact with a flexible vessel wall.

*Microparticles at ACT<sup>®</sup> bubble surface.* Some of the ACT<sup>®</sup> bubbles occasionally had microparticles attached to their surface, which might be microdroplets not forming microclusters. During oscillations and in the process of collapsing, a jet seemed to protrude through the bubble, and the attached microparticles were shot away from the ACT<sup>®</sup> bubbles (Fig. 12). This transport of microparticles was recorded at a lower rate of 15 fps (Video S6, online only). The rapid movement of the microparticles away from the ACT<sup>®</sup> bubble was not seen in the short duration of the high-rate recording. During the 17- $\mu\text{s}$  ultrahigh-speed movie, the particles remained in contact with the ACT<sup>®</sup> bubbles, and transport of the microbubbles should not be observed. The observation is interesting, but delivery of micro-nanoparticles in contact with the oscillating ACT<sup>®</sup> bubble probably occurs rather seldomly to be an important transport mechanism.

*Shear stress.* The oscillating microbubble will, when in the proximity of a solid boundary, cause an oscillatory shear stress on the solid boundary. Figure 13 illustrates the estimated oscillatory shear stresses obtained from optical observations of 10 different ACT<sup>®</sup> bubbles. The drive frequency used was 500 kHz, and three different acoustic pressures were tested (127, 191 and 254 kPa). The resulting shear stress increases linearly with the displacement amplitude of the bubble according to eqn (4). The displacement amplitude for the oscillating ACT<sup>®</sup> bubbles was similar to that reported for regular contrast agent microbubbles (Helfield et al. 2016a, 2016b); thus, the local shear stress

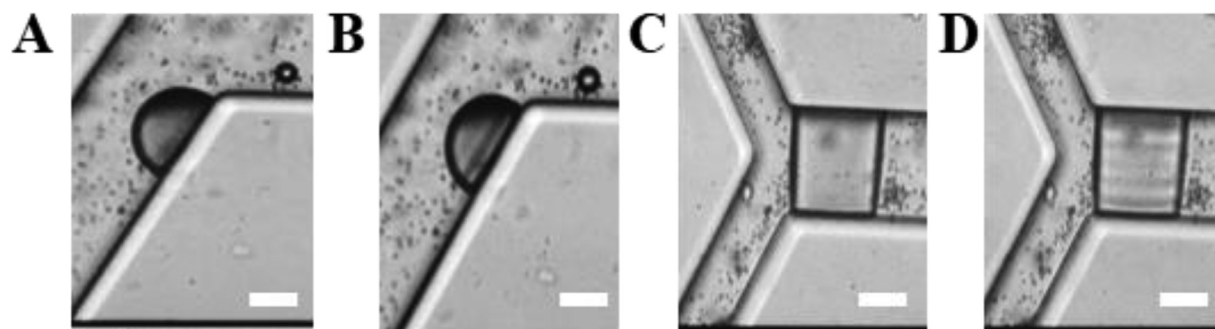


Fig. 11. Surface rippling on half-circle and square microbubbles. (A, C) Before ultrasound burst. (B, D) “Surface” wave travels “through” the half-circle bubble and square bubble. One-megahertz ultrasound at 400 kHz. Bar = 25  $\mu\text{m}$ .

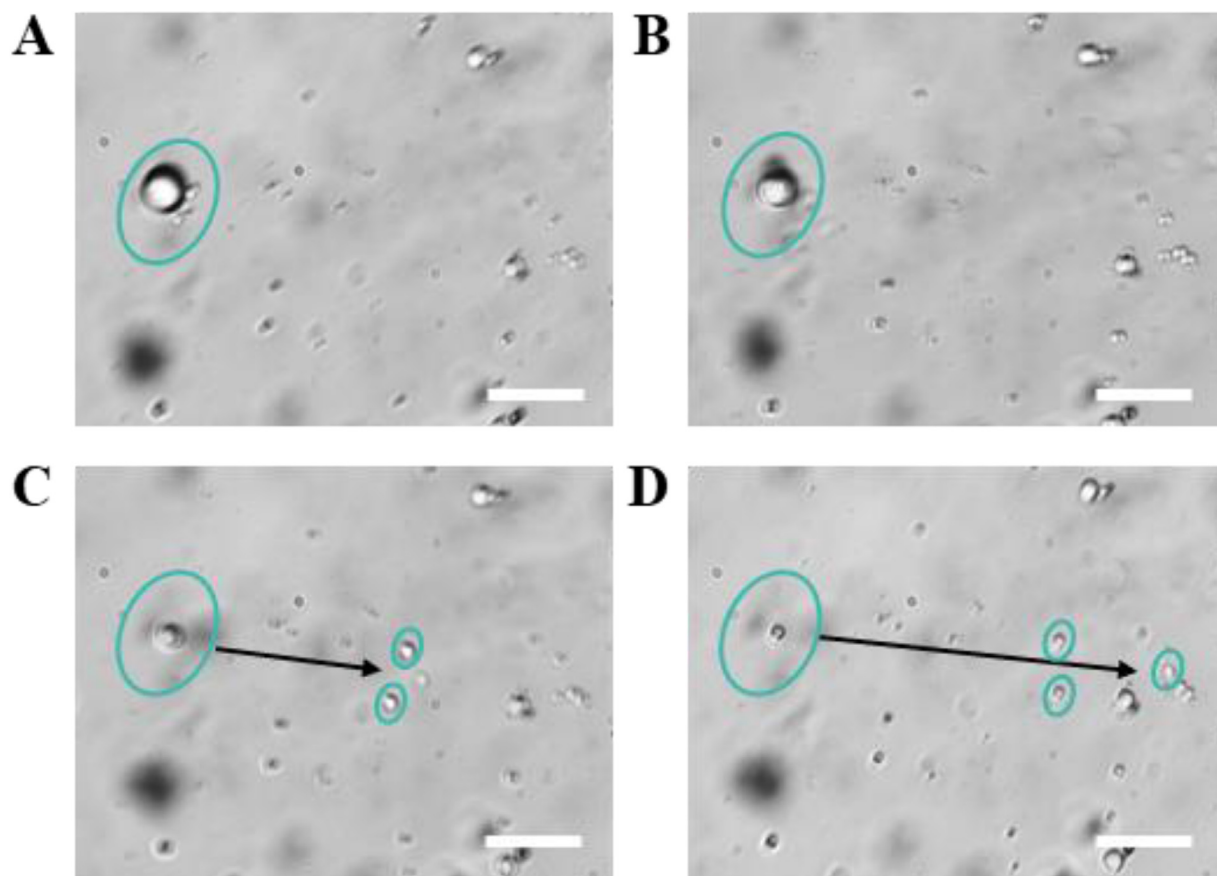


Fig. 12. Selected frames of a 13- $\mu\text{m}$  ACT bubble surrounded by three microparticles with diameters of 2.2, 2.8 and 3.0  $\mu\text{m}$ . After a 0.5-MHz ultrasound burst of 8 cycles at 127 kPa, the microparticles shoot off the ACT bubble to the right. They kept on moving until the end of the video, which lasted 14 s from the ultrasound burst. The smallest particle reached the furthest point (114.8  $\mu\text{m}$ ) from the bubble, and the other two reached approximately 81.6  $\mu\text{m}$ . The ACT bubble had shrunk in size to 3  $\mu\text{m}$ . Bar = 25  $\mu\text{m}$ . ACT = Acoustic Cluster Therapy.

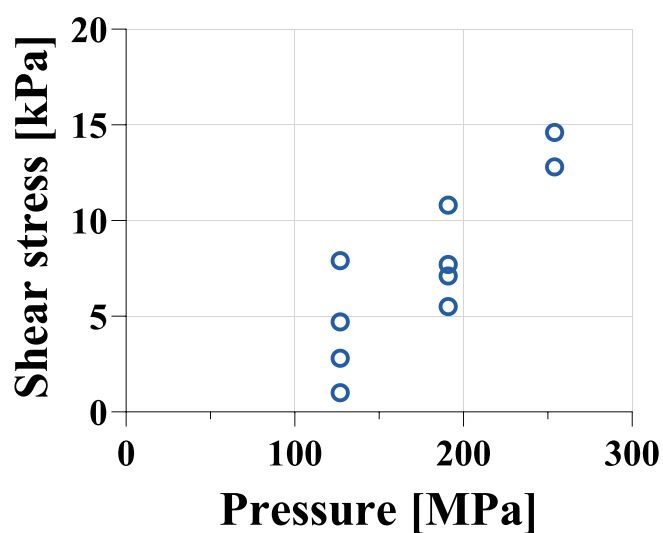


Fig. 13. Estimated oscillatory shear stress at solid boundary obtained from optical observations of 10 different ACT bubbles exposed to 500-kHz ultrasound at three different pressures: 127, 191 and 254 kPa. ACT = Acoustic Cluster Therapy.

will be of the same order. However, as the ACT<sup>®</sup> bubbles cover a larger area than the smaller microbubbles, the area exposed to the shear stress is larger.

## CONCLUSIONS

Activation of microclusters resulting in large ACT<sup>®</sup> bubbles was initiated by fusion of the microbubble–microdroplet, followed by vaporization of the microdroplet and an inward diffusion of gas. The ACT<sup>®</sup> bubbles oscillated according to the modified Rayleigh–Plesset equation when a term accounting for thermal damping and a term accounting for boundary conditions imposed by the microchannel wall were included. The changes in ACT<sup>®</sup> bubble radii during oscillations amounted to 1–2  $\mu\text{m}$ , similar to those for commercial contrast agent microbubbles. However, the volume of ACT<sup>®</sup> bubbles was much larger; thus, the ACT<sup>®</sup> bubbles can be in direct contact with a larger part of the microchannel wall, as well as block the smaller channels. The previously reported promising therapeutic responses in mice treated with ACT<sup>®</sup> and various drugs suggest that the ACT<sup>®</sup> bubble oscillations along a segment of the capillary wall can improve drug delivery. The optimal frequencies for the activation step and enhancement step are different, and therefore, both are necessary for effective delivery of drugs and enhanced therapeutic response.

This is the first time the activation and oscillations of ACT<sup>®</sup> bubbles have been imaged in microchannels, and the observations of activation and oscillation of ACT<sup>®</sup> bubbles support previously findings. Although the observations were made in an environment different from that in capillaries, these data provide new insight into the dynamics of ACT<sup>®</sup> bubble activation and oscillations.

## DECLARATION OF COMPETING INTEREST

A.H. is CEO of EXACT Therapeutics. The other authors declare no conflicts of interest.

*Acknowledgments*—The project was funded by The Research Council of Norway under Nano2021 Project No. 262228. F.S.V. and X.C. were partially supported by a grant from the National Institutes of Health (R01 EB026966). Illustrations were created with BioRender.com.

## SUPPLEMENTARY MATERIALS

Supplementary material associated with this article can be found in the online version at [doi:10.1016/j.ultrasmedbio.2022.05.009](https://doi.org/10.1016/j.ultrasmedbio.2022.05.009).

## REFERENCES

Abou-Saleh RH, Peyman SA, Johnson BRG, Marston G, Ingram N, Bushby R, Coletta PL, Markham AF, Evans SD. The influence of

- intercalating perfluorohexane into lipid shells on nano and microbubble stability. *Soft Matter* 2016;12:7223–7230.
- Alrifaiy A, Lindahl OA, Ramser K. Polymer-based microfluidic devices for pharmacy, biology and tissue engineering. *Polymers* 2012;4:1349–1398.
- Aslund AK, Snipstad S, Healey A, Kvale S, Torp SH, Sontum PC, Davies CL, van Wamel A. Efficient enhancement of blood–brain barrier permeability using Acoustic Cluster Therapy (ACT). *Theranostics* 2017;7:23–30.
- Bouakaz A, Versluis M, de Jong N. High-speed optical observations of contrast agent destruction. *Ultrasound Med Biol* 2005;31:391–399.
- Boucher Y, Jain RK. Microvascular pressure is the principal driving force for interstitial hypertension in solid tumors: Implications for vascular collapse. *Cancer Res* 1992;52:5110–5114.
- Brujan EANK, Schmidt P, Vogel A. Dynamics of laser-induced cavitation bubbles near an elastic boundary used as a tissue phantom. *J Fluid Mech* 2000;433:251–281.
- Bush N, Healey A, Shah A, Box G, Kirkin V, Eccles S, Sontum PC, Kotopoulos S, Kvale S, van Wamel A, Davies CL, Bamber J. Therapeutic attributes of acoustic cluster therapy and its use for enhancing the effectiveness of liposomal doxorubicin treatment of human triple negative breast cancer in mice. *Front Pharmacol* 2020;11:75.
- Caskey CF, Stieger SM, Qin S, Dayton PA, Ferrara KW. Direct observations of ultrasound microbubble contrast agent interaction with the microvessel wall. *J Acoust Soc Am* 2007;122:1191–1200.
- Chen H, Brayman AA, Bailey MR, Matula TJ. Blood vessel rupture by cavitation. *Proc IEEE Int Ultrason Symp* 2010;678–681.
- Chen H, Brayman AA, Evan AP, Matula TJ. Preliminary observations on the spatial correlation between short-burst microbubble oscillations and vascular bioeffects. *Ultrasound Med Biol* 2012;38:2151–2162.
- Chen X, Wang J, Versluis M, de Jong N, Villanueva FS. Ultra-fast bright field and fluorescence imaging of the dynamics of micrometer-sized objects. *Rev Sci Instrum* 2013;84 063701.
- Delalande A, Kotopoulos S, Postema M, Midoux P, Pichon C. Sonoporation: Mechanistic insights and ongoing challenges for gene transfer. *Gene* 2013;525:191–199.
- Delalande A, Bastie C, Pigeon L, Manta S, Lebertre M, Mignet N, Midoux P, Pichon C. Cationic gas-filled microbubbles for ultrasound-based nucleic acids delivery. *Biosci Rep* 2017;37 BSR20160619.
- Dimcevski G, Kotopoulos S, Bjanec T, Hoem D, Schjott J, Gjertsen BT, Biermann M, Molven A, Sorbye H, McCormack E, Postema M, Gilja OH. A human clinical trial using ultrasound and microbubbles to enhance gemcitabine treatment of inoperable pancreatic cancer. *J Control Release* 2016;243:172–181.
- Doinikov AA, Zhao S, Dayton PA. Modeling of the acoustic response from contrast agent microbubbles near a rigid wall. *Ultrasonics* 2009;49:195–201.
- Eatock BC, Nishi RY, Johnston GW. Numerical studies of the spectrum of low-intensity ultrasound scattered by bubbles. *J Acoustic Soc Am* 1985;77:1692–1701.
- Gac SL, Zwaan E, van den Berg A, Ohl CD. Sonoporation of suspension cells with a single cavitation bubble in a microfluidic confinement. *Lab Chip* 2007;7:1666–1672.
- Goertz DE. An overview of the influence of therapeutic ultrasound exposures on the vasculature: High intensity ultrasound and microbubble-mediated bioeffects. *Int J Hyperthermia* 2015;31:134–144.
- Healey AJ, Sontum PC, Kvale S, Eriksen M, Bendiksen R, Tornes A, Ostensen J. Acoustic cluster therapy: In vitro and ex vivo measurement of activated bubble size distribution and temporal dynamics. *Ultrasound Med Biol* 2016;42:1145–1166.
- Helfield B, Black JJ, Qin B, Pacella J, Chen X, Villanueva FS. Fluid Viscosity affects the fragmentation and inertial cavitation threshold of lipid-encapsulated microbubbles. *Ultrasound Med Biol* 2016a;42:782–794.
- Helfield B, Chen X, Watkins SC, Villanueva FS. Biophysical insight into mechanisms of sonoporation. *Proc Natl Acad Sci USA* 2016b;113:9983–9988.

- Husseini GA, Pitt WG, Martins AM. Ultrasonically triggered drug delivery: Breaking the barrier. *Colloids Surf B Biointerfaces* 2014;123:364–386.
- Ingram N, McVeigh LE, Abou-Saleh RH, Maynard J, Peyman SA, McLaughlan JR, Fairclough M, Marston G, Valleley EMA, Jimez-Macias JL, Charalambous A, Townley W, Haddrick M, Wierzbicki A, Wright A, Volpato M, Simpson PB, Treanor DE, Thomson NH, Loadman PM, Bushby RJ, Johnson BRG, Jones PF, Evans JA, Freear S, Markham AF, Evans SD, Coletta PL. Ultrasound-triggered therapeutic microbubbles enhance the efficacy of cytotoxic drugs by increasing circulation and tumor drug accumulation and limiting bioavailability and toxicity in normal tissues. *Theranostics* 2020;10:10973–10992.
- Johnston ID, McCluskey DK, Tan CKL, Tracey MC. Mechanical characterization of bulk Sylgard 184 for microfluidics and microengineering. *J Micromech Microeng* 2014;24:17.
- Kooiman K, Vos HJ, Versluis M, de Jong N. Acoustic behavior of microbubbles and implications for drug delivery. *Adv Drug Deliv Rev* 2014;72:28–48.
- Kotopoulos S, Stigen E, Popa M, Safont MM, Healey A, Kvale S, Sontum P, Gjertsen BT, Gilja OH, McCormack E. Sonoporation with Acoustic Cluster Therapy (ACT<sup>®</sup>) induces transient tumour volume reduction in a subcutaneous xenograft model of pancreatic ductal adenocarcinoma. *J Control Release* 2017;245:70–80.
- Lajoinie G, De Cock I, Coussios CC, Lentacker I, Le Gac S, Stride E, Versluis M. In vitro methods to study bubble–cell interactions: Fundamentals and therapeutic applications. *Biomicrofluidics* 2016;10 011501.
- Lee H, Kim H, Han H, Lee M, Lee S, Yoo H, Chang JH, Kim H. Microbubbles used for contrast enhanced ultrasound and thernagnosis: A review of principles to applications. *Biomed Eng Lett* 2017;7:59–69.
- Lentacker I, De Cock I, Deckers R, De Smedt SC, Moonen CT. Understanding ultrasound induced sonoporation: Definitions and underlying mechanisms. *Adv Drug Deliv Rev* 2014;72:49–64.
- Medwin H. Counting bubbles acoustically—Review. *Ultrasonics* 1977;15:7–13.
- Myhre O, Bjorgan M, Grant D, Hustvedt SO, Sontum PC, Dirven H. Safety assessment in rats and dogs of Acoustic Cluster Therapy, a novel concept for ultrasound mediated, targeted drug delivery. *Pharmacol Res Perspect* 2016;4:e00274.
- Olsman M, Muhlenpfordt M, Olsen EB, Torp SH, Kotopoulos S, Rijcken CJF, Hu Q, Thewissen M, Snipstad S, de Lange Davies C. Acoustic Cluster Therapy (ACT<sup>®</sup>) enhances accumulation of polymeric micelles in the murine brain. *J Control Release* 2021;337:285–295.
- Plesset MS. The dynamics of cavitation bubbles. *J Appl Mech* 1949;16:277–282.
- Poon C, McMahon D, Hynynen K. Noninvasive and targeted delivery of therapeutics to the brain using focused ultrasound. *Neuropharmacology* 2017;120:20–37.
- Postema M, van Wamel A, Lancee CT, de Jong N. Ultrasound-induced encapsulated microbubble phenomena. *Ultrasound Med Biol* 2004;30:827–840.
- Pulsipher KW, Hammer DA, Lee D, Sehgal CM. Engineering therapeutic microbubbles using microfluidics for ultrasound imaging and therapy: A review. *Ultrasound Med Biol* 2018;44:2441–2460.
- Qin P, Han T, Yu ACH, Xu L. Mechanistic understanding the bioeffects of ultrasound-driven microbubbles to enhance macromolecule delivery. *J Control Release* 2018;272:169–181.
- Rayleigh LVIII. On the pressure developed in a liquid during the collapse of a spherical cavity. *Philos Mag* 1917;34:94–98.
- Roovers S, Segers T, Lajoinie G, Deprez J, Versluis M, De Smedt SC, Lentacker I. The role of ultrasound-driven microbubble dynamics in drug delivery: From microbubble fundamentals to clinical translation. *Langmuir* 2019;35:10173–10191.
- Snipstad S, Berg S, Morch Y, Bjorkoy A, Sulheim E, Hansen R, Grimstad I, van Wamel A, Maaland AF, Torp SH, Davies CL. Ultrasound improves the delivery and therapeutic effect of nanoparticle-stabilized microbubbles in breast cancer xenografts. *Ultrasound Med Biol* 2017;43:2651–2669.
- Sontum P, Kvale S, Healey AJ, Skurtveit R, Watanabe R, Matsumura M, Ostensen J. Acoustic Cluster Therapy (ACT)—A novel concept for ultrasound mediated, targeted drug delivery. *Int J Pharm* 2015;495:1019–1027.
- Stride E, Segers T, Lajoinie G, Cherkaoui S, Bettinger T, Versluis M, Borden M. Microbubble agents: New directions. *Ultrasound Med Biol* 2020;46:1326–1343.
- Su YC. MEMS packaging. Hackensack, NJ: World Scientific; 2018.
- Tung YS, Marquet F, Teichert T, Ferrera V, Konofagou EE. Feasibility of noninvasive cavitation-guided blood–brain barrier opening using focused ultrasound and microbubbles in nonhuman primates. *Appl Phys Lett* 2011;98 163704.
- Tzu-Yin W, Wilson KE, Machtaler S, Willmann JK. Ultrasound and microbubble guided drug delivery: Mechanistic understanding and clinical implications. *Curr Pharm Biotechnol* 2013;14:743–752.
- van der Meer SM, Dollet B, Voormolen MM, Chin CT, Bouakaz A, de Jong N, Versluis M, Lohse D. Microbubble spectroscopy of ultrasound contrast agents. *J Acoust Soc Am* 2007;121:648–656.
- van Wamel V, Healey A, Sontum PC, Kvale S, Bush N, Bamber J, de Lange Davies C. Acoustic Cluster Therapy (ACT)—Pre-clinical proof of principle for local drug delivery and enhanced uptake. *J Control Release* 2016a;224:158–164.
- van Wamel A, Sontum PC, Healey A, Kvale S, Bush N, Bamber J, de Lange Davies C. Acoustic Cluster Therapy (ACT) enhances the therapeutic efficacy of paclitaxel and Abraxane<sup>®</sup> for treatment of human prostate adenocarcinoma in mice. *J Control Release* 2016b;236:15–21.
- Versluis M, Stride E, Lajoinie G, Dollet B, Segers T. Ultrasound contrast agent modeling: A review. *Ultrasound Med Biol* 2020;46:2117–2144.
- Wang S, Hossack JA, Klibanov AL. Targeting of microbubbles: Contrast agents for ultrasound molecular imaging. *J Drug Target* 2018;26:420–434.
- Wang SP, Wang QX, Zhang AM, Stride E. Experimental observations of the behaviour of a bubble inside a circular rigid tube. *Int J Multiphas Flow* 2019;121.
- Yan F, Li L, Deng Z, Jin Q, Chen J, Yang W, Yeh CK, Wu J, Shandas R, Liu X, Zheng H. Paclitaxel–liposome–microbubble complexes as ultrasound-triggered therapeutic drug delivery carriers. *J Control Release* 2013;166:246–255.
- Yang Y, Li Q, Guo X, Tu J, Zhang D. Mechanisms underlying sonoporation: Interaction between microbubbles and cells. *Ultrason Sonochem* 2020;67 105096.
- Yeh CK, Su SY. Effects of acoustic insonation parameters on ultrasound contrast agent destruction. *Ultrasound Med Biol* 2008;34:1281–1291.